Pergamon

Geochimica et Cosmochimica Acta, Vol. 67, No. 9, pp. 1711–1721, 2003

0016-7037/03 $30.00 + .00

doi:10.1016/S0016-7037(02)01172-9

Fine-grained-rim mineralogy of the Cold Bokkeveld CM chondrite

THOMAS J. ZEGA[1,*] and PETER R. BUSECK[1,2]

[1]Department of Geological Sciences, Arizona State University, Tempe, AZ 85287–1404, USA
[2]Department of Chemistry and Biochemistry, Arizona State University, Tempe, AZ 85287–1404, USA

(*Received December* 7, 2001; *accepted in revised form August* 27, 2002)

Abstract—A chrysotile-like phase, cronstedtite, polygonal serpentine, pentlandite, and finely intergrown tochilinite comprise the fine-grained rim (FGR) mineralogy of the Cold Bokkeveld CM chondrite. Transmission electron microscope images combined with compositional data indicate reaction among cronstedtite, the chrysotile-like phase, and polygonal serpentine. The Mg/(Mg+Fe) ratios of the cronstedtite are higher than those reported for the less altered Murchison CM chondrite. Cronstedtite grains exhibit layer separations, particularly at their boundaries.

The FGRs surround different chondrule types but have similar bulk compositions and mineralogy. Ca is depleted in the FGRs relative to the bulk CM chondrite. The FGRs display non-uniform thicknesses, especially where they coat embayed chondrule areas, and they exhibit grain-size coarsening outward from the chondrules they enclose. FGR formation in Cold Bokkeveld is most plausibly explained by multiple accretionary episodes during which progressively coarser dust was deposited onto chondrules, presumably in the solar nebula. The compositional and mineralogic data are consistent with aqueous alteration on the parent body. *Copyright © 2003 Elsevier Science Ltd*

1. INTRODUCTION

The CM chondrites are among the oldest and most primitive materials available for study and contain information of events that transpired in the early solar system. They consist of mixtures that include coarse-grained (several millimeters down to hundreds of microns) components such as Ca- and Al-rich inclusions (CAIs) and chondrules that are surrounded by fine-grained rim (FGR) and matrix material. This material is of interest because its high surface area provides abundant reaction sites, making it a sensitive recorder of chemical processes.

The fine-grained texture and enveloping form of the FGRs are intriguing, prompting questions regarding their formation. The rims of the CM chondrites are particularly interesting because of their extremely small grain sizes and apparent primitive origin. Several models have been proposed for the formation of the FGRs in CM chondrites. These include: (1) accretion of both hydrous and anhydrous dust onto coarse-grained components such as chondrules and CAIs (Bunch and Chang, 1984; Metzler et al., 1992; Metzler and Bischoff, 1997; Bischoff, 1998), (2) accretion of material onto coarse-grained components in the solar nebula and aqueous alteration on a meteorite parent body (Brearley and Geiger, 1991; Zolensky et al., 1993; Brearley et al., 1999; Hanowski and Brearley, 2001; Hua et al., 2002), and (3) aqueous alteration of coarse-grained components in a parent-body regolith (Sears et al., 1992, 1993). However, after two decades of debate, no consensus exists regarding the origin of these rims.

The high-resolution and analytical capabilities provided by transmission electron microscopy (TEM) have allowed detailed mineralogic investigations of fine-grained meteoritic materials. Brearley and Geiger (1991, 1993), Buseck et al. (1997), Li et al. (1999), Brearley et al. (1999), and Lauretta et al. (2000) used TEM to determine the FGR mineralogy of the Murchison, ALH 81002, and LEW 90500 CM chondrites. Here we expand on those efforts by reporting new findings from FGRs around chondrules in the Cold Bokkeveld CM chondrite. Prior results were reported by Zega and Buseck (2000, 2001).

Cold Bokkeveld was selected because it contains abundant FGRs, is one of the most altered CM chondrites (Browning et al., 1996), and is a fall. Examination of Cold Bokkeveld therefore permits observation of the effects of intense alteration on FGR material. We also compare our observations to the less altered Murchison and ALH 81002 CM chondrites to gain an understanding of the effects of increased alteration on FGR mineralogy.

2. SAMPLES AND ANALYTICAL METHODS

Three petrographic thin sections of Cold Bokkeveld were surveyed using reflected- and transmitted-light optical microscopy and scanning electron microscopy. We identified more than 25 FGRs and selected four that surround chondrules for detailed investigation. Metzler et al. (1992) showed that Cold Bokkeveld is slightly brecciated and contains lithic fragments that range in size from ~100 μm to several centimeters. The chondrule-FGR assemblages that we chose for detailed investigation come from a fragment that shows no appreciable sign of brecciation.

FGR compositions were measured using a JEOL JXA8600 electron microprobe with a broad (50 μm) beam operated at 15 keV and 10 nA. We acquired five to 15 analyses per rim (depending on rim thickness), avoiding overlapping analyses and inclusion of chondrule or matrix material. Wavelength dispersive spectrometers were calibrated for Na, Mg, Al and Si, P, S, K, Ca, Ti, Cr, Mn, Fe, and Ni using albite, periclase, anorthite, apatite, barite, orthoclase, wollastonite, rutile, chromite, rhodonite, synthetic wüstite, and NiO standards, respectively. Oxide compositions were determined from stoichiometry based on 24 oxygen atoms per formula unit. A 30-s count time and standard ZAF-correction procedure were employed for each analysis. Textural features of FGRs and chondrules were examined using a JEOL-840 scanning electron microscope (SEM) and Hitachi S-4700 field-emission gun SEM (FEG-SEM).

We mounted Cu-ring supports onto the selected assemblages using M-bond 610 (M-line Accessories and Measurements Group), an ace-

* Author to whom correspondence should be addressed (tzega@asu.edu).

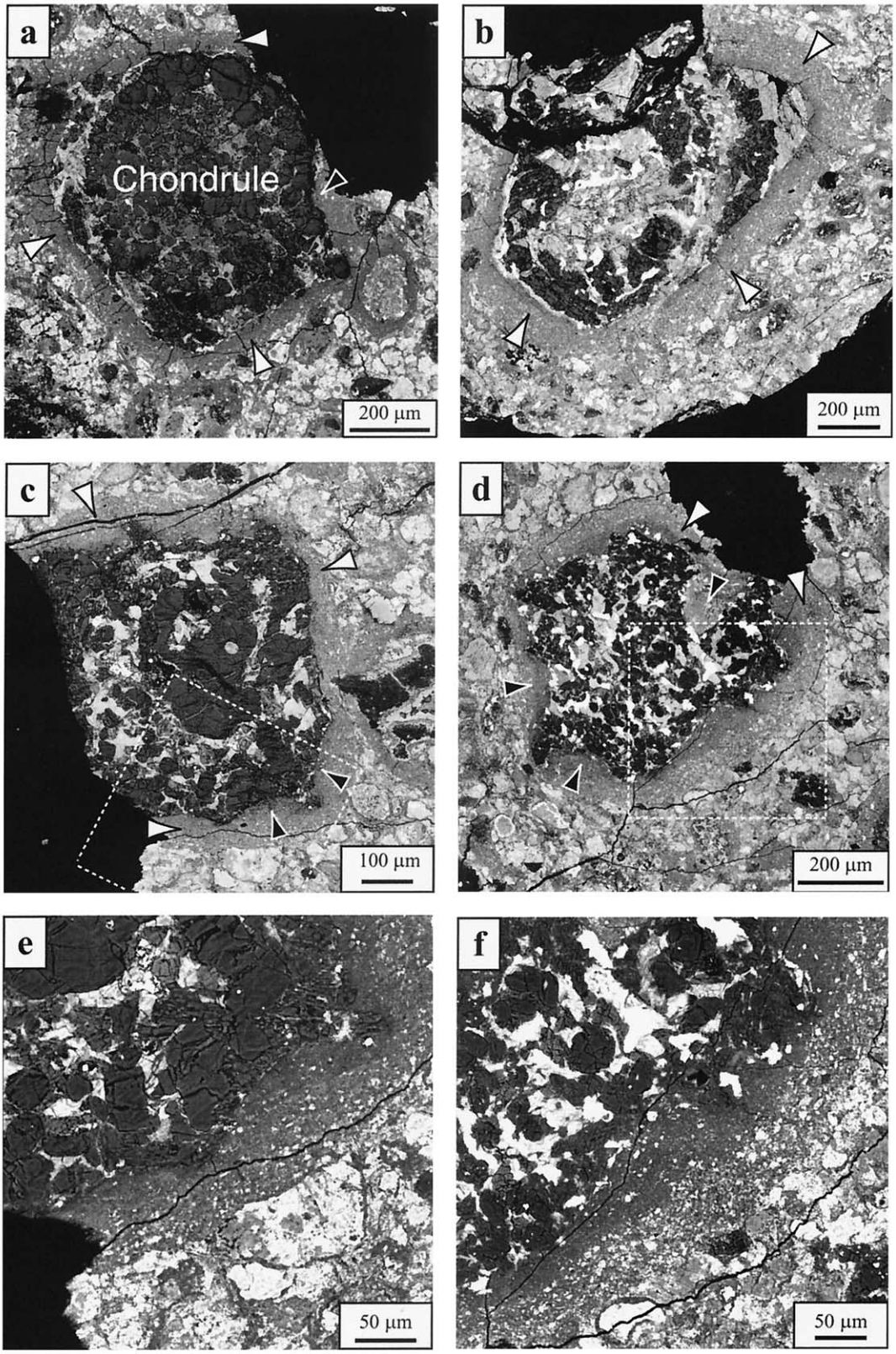

Fig. 1. (a–d) Back-scattered SEM images of the four studied FGRs (white arrowheads). Embayed chondrule areas contain fine-grained material (black arrowheads). Chondrule types are as follows: a = IA, b = IB, c =IAB, d = IIAB. (e,f) Higher magnification images of the areas delineated by the white boxes in (c) and (d), respectively, exhibiting grain-size coarsening outward from the chondrules.

Table 1. Average FGR compositions (wt.%) from broad-beam (50 μm) electron microprobe analyses.*

	FGR #			
Oxide	1 (5)	2 (9)	3 (8)	4 (15)
Na_2O	0.48 *0.1*	0.48 *0.1*	0.50 *0.1*	0.47 *0.1*
MgO	16.5 *1.2*	21.6 *2.1*	17.7 *2.5*	19.8 *2.3*
Al_2O_3	1.48 *0.2*	1.42 *0.3*	1.69 *0.5*	1.81 *0.5*
SiO_2	30.2 *1.7*	31.8 *2.8*	31.2 *3.0*	32.0 *2.7*
P_2O_5	0.33 *0.07*	0.53 *0.4*	0.32 —	0.71 *0.06*
SO_3	3.94 *0.3*	3.69 *0.6*	4.13 *0.8*	3.79 *1.2*
K_2O	BMDL —	BMDL —	BMDL —	BMDL —
CaO	0.18 *0.1*	0.48 *0.4*	0.28 *0.1*	0.35 *0.4*
TiO_2	0.10 *0.01*	0.10 *0.02*	0.11 *0.02*	0.10 *0.02*
Cr_2O_3	0.61 *0.03*	0.69 *0.2*	0.67 *0.2*	0.70 *0.09*
MnO	0.28 *0.02*	0.25 *0.01*	0.28 *0.03*	0.28 *0.03*
FeO	18.9 *0.7*	21.1 *5.2*	22.7 *4.8*	23.8 *7.4*
NiO	2.55 *0.4*	2.73 *0.7*	2.92 *1.3*	2.39 *1.1*
TOTAL	75.5	84.9	82.5	86.2

* Number of analyses performed is in parentheses. Numbers in italics indicate the standard deviations. BMDL = below minimum detection level.

tone-insoluble adhesive. After curing, the material around each Cu ring was removed using a carbide microtool, and the entire thin section was immersed in acetone for 1 h to dissolve the thin-section adhesive. The assemblages of interest, with Cu-ring supports attached, were then extracted and thinned to electron transparency using a Gatan™ precision ion-polishing system (PIPS). The PIPS was operated at a constant 3-rpm rotation rate and a varied acceleration voltage (5.0 to 2.5 keV) and Ar-ion bombardment angle (6.0 to 2.5°).

The FGR assemblages were examined using high-resolution TEM (HRTEM) and selected-area electron diffraction (SAED) with a 200-keV JEOL 2000FX (C_s = 2.0 mm) transmission electron microscope equipped for energy dispersive spectrometry (EDS) and a 400-keV JEOL 4000EX transmission electron microscope (C_s = 1.0 mm). Mineral identifications were based on electron-diffraction patterns and chemical analyses using experimentally determined k-factors (Cliff and Lorimer, 1975; Van Cappellen and Doukhan, 1994). Computer-simulated HRTEM images were generated using Cerius$^{2©}$ V4.0 (Molecular Simulations), and image processing was performed with Adobe Photoshop® and Gatan DigitalMicrograph™.

3. PETROLOGY AND MINERALOGY

The studied FGRs (Fig. 1) surround types IA, IB, IAB, and IIAB chondrules. The average compositions of the rims are similar to one another (Table 1) and display similar abundance patterns when normalized to Si and the bulk CM (Fig. 2). The FGRs are depleted in Ca (ranging from a factor of 4.2 to 10.7) relative to the bulk CM (Kerridge and Matthews, 1988). The depletion of Ca has been observed in the FGRs of most CM chondrites (Metzler et al., 1992; Hua et al., 2002) and also some CV (Hua et al., 1996) and CO chondrites (Brearley, 1993; Brearley et al., 1995). S is slightly depleted (by a factor of 2.5), and P is slightly enriched for two of the FGRs (by a factor of 2.2 to 3.0) relative to the bulk CM.

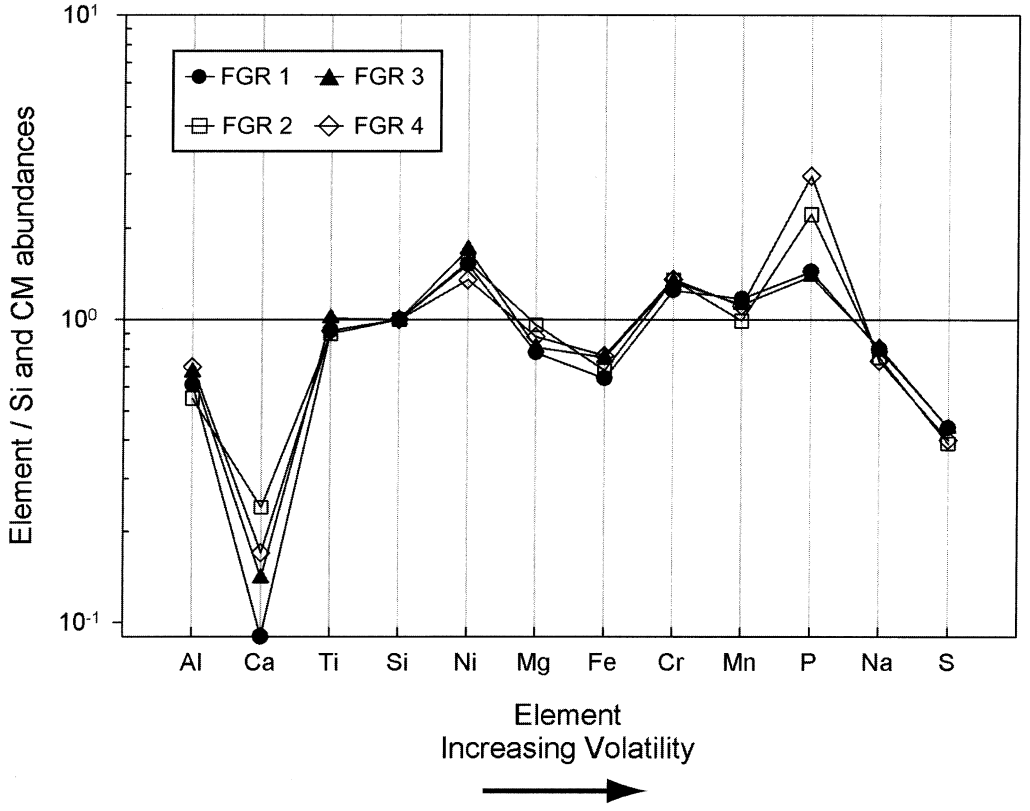

Fig. 2. Average compositions of Cold Bokkeveld FGRs from electron microprobe analyses. Weight percentages are shown for major elements in order of increasing volatility (decreasing condensation temperature) normalized to Si and the bulk CM chondrite composition (Kerridge and Matthews, 1988).

The rims exhibit non-uniform widths, filling embayed areas of the chondrules (Fig. 1a–d). Some rims show layering and exhibit grain-size coarsening outward from the chondrule (Fig. 1e,f). Textures show that the FGRs are intact, indicating they did not experience brecciation after formation. The chondrule and FGR contacts are sharp, and the FEG-SEM images show altered silicate and sulfide grains in the chondrules. All the FGRs we studied contain a chrysotile-like phase, pentlandite, cronstedtite, polygonal serpentine, and serpentine-tochilinite intergrowths. Grain morphologies, sizes, and relative abundances are listed in Table 2.

The chrysotile-like phase is the main mineral of the FGRs. It has a round (Fig. 3a), fibrous morphology containing layers separated by 0.7 nm and is rich in Mg, although it contains high amounts of Fe for a Mg silicate (Table 3). We infer that these grains are cylinders in projection, similar to chrysotile but with higher Fe content, which is why we call them chrysotile-like. Most grains range from 15 to 30 nm across, although some adjacent to cronstedtite are ~150 nm across. Euhedral to subhedral pentlandite occurs scattered throughout the chrysotile-like regions (Fig. 3b). Serpentine-tochilinite intergrowths occur between some chrysotile-like grains and pentlandite. These intergrowths are poorly crystalline and exhibit both straight and curled morphologies (Fig. 3c).

Cronstedtite occurs between the regions containing the chrysotile-like phase and pentlandite (Fig. 4). The cronstedtite has a platy morphology and stacking disorder. Some grains appear highly disordered and contain almost no layer continuity (Fig. 4), but even well-ordered grains contain kinks and dislocations (Fig. 5). The layers of some cronstedtite grains separate at their boundaries by bending or curling away from the (001) plane and into the chrysotile-like phase or polygonal serpentine (Fig. 6). In other instances, the chrysotile-like phase pseudomorphically replaces cronstedtite (Fig. 4).

We simulated HRTEM images of cronstedtite to interpret the contrast features exhibited in some of the grains. Using 1*T*, $2H_2$, and 3*T* structure models (Geiger et al., 1983; Smrcok et al., 1994; Hybler et al., 2000), we found a plausible match between the experimental and simulated images (Fig. 7) for the 1*T* polytype.

The cronstedtite in the Cold Bokkeveld FGRs contains between 2.7 and 8.8 at % Mg, which is consistent with the range of $<$ 1 to 16.4 at % Mg reported for terrestrial and meteoritic cronstedtite (Müller et al., 1979; Smrcok et al., 1994; Lauretta et al., 2000). All cronstedtite grains contain Al, but we did not observe Mn even though it is common in terrestrial crystals. Nine of 22 analyzed grains contain between 0.4 and 1.5 at % S, which is less than the 4.4 at % S in Murchison and Mighei cronstedtite (Tomeoka and Buseck, 1985). The Mg/(Mg+Fe) ratios of three FGRs are 0.21(± 0.06), 0.25(± 0.08), and 0.32(± 0.15). A ratio of 0.44 was obtained from a grain in the fourth FGR. All lie within the 0.0 to 0.4 range reported for terrestrial and meteoritic cronstedtite (Müller et al., 1979; Smrcok et al., 1994; Brearley et al., 1999; Lauretta et al., 2000).

Polygonal serpentine occurs in low abundance within the chrysotile-like phase. However, the polygonal material is typically coarser grained and exhibits a characteristic bowtie diffraction contrast (Fig. 8) similar to 30-sectored terrestrial polygons in off-axis orientation (Dodony, 1997). Most grains exhibit layer separations both near and between sector bound-

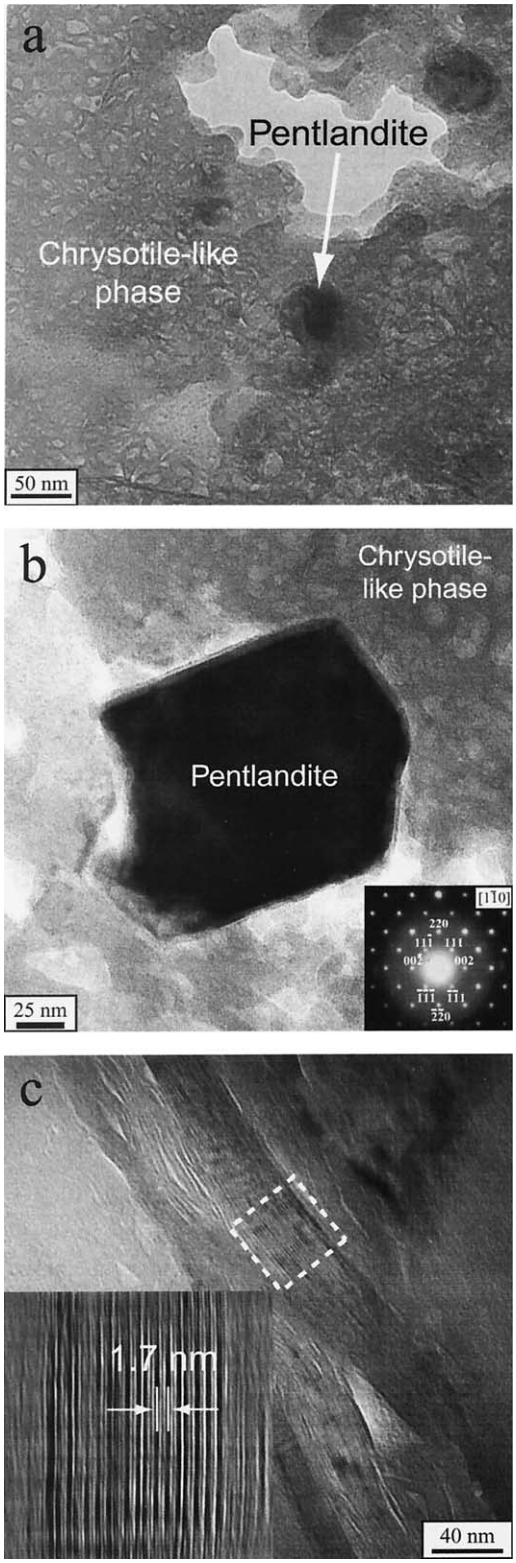

Fig. 3. (a) TEM image of a region containing the chrysotile-like phase and pentlandite. (b) Pentlandite occurs within the finer-grained chrysotile-like phase. Inset SAED pattern is of pentlandite. (c) Poorly crystalline region containing a serpentine-tochilinite intergrowth. Inset image shows the layer periodicity of 1.7 nm.

Table 2. Chemistry, morphology, and dimensions of Cold Bokkeveld FGR minerals.*

Mineral	Ideal Formula	Morphology	Dimensions (nm)
Chrysotile-like	$Mg_3Si_2O_5(OH)_4$	round	15 to 150
Cronstedtite	$Fe^{2+}_{3-x}Fe^{3+}_x[Si_{2-x}Fe^{3+}_xO_5](OH)_4$ $0 < x < 1$	platy	25 to 400
Pentlandite	$(Fe,Ni)_9S_8$	euhedral to subhedral	50 to 250
Tochilinite	$6FeS \cdot 5[(Fe,Mg)(OH)_2]$	straight and curled	30 to 50
Polygonal Serpentine	$Mg_3Si_2O_5(OH)_4$	round with sectors	200 to 750

* Listed in order of relative abundance (most to least from top to bottom, respectively).

aries (Fig. 8). Polygonal serpentine contains between 0.9 and 3.7 at % Fe, which is within the 1.0 to 6.4 at % range reported for its terrestrial counterpart (Wicks and Plant, 1979).

4. DISCUSSION

4.1. Mineralogy

Cronstedtite, the chrysotile-like phase, and polygonal serpentine are characteristically associated. Where adjacent, the (001) cronstedtite layers are continuous with the chrysotile-like phase and polygonal serpentine (Fig. 6). We infer that this layer continuity indicates a structural transformation among the three phases. The EDS measurements indicate deviation from endmember compositions (Fig. 9), and the data scatter along the line connecting cronstedtite and chrysotile compositions. We infer from the TEM data and EDS measurements that a relation exists between cronstedtite and serpentine, i.e.

$$\underset{\text{(cronstedtite)}}{Fe^{2+}_{2.5}Fe^{3+}_{0.5}[Si_{1.5}Fe^{3+}_{0.5}O_5](OH)_4} + 3Mg^{2+} + 0.5Si^{4+} \leftrightarrow \underset{\text{(serpentine)}}{Mg_3Si_2O_5(OH)_4} + 2.5Fe^{2+} + Fe^{3+} \quad (1)$$

This idealized reaction is based on endmember compositions and involves a site-specific coupled exchange. Fe^{2+} and Mg^{2+} can substitute for one another in octahedral sites, whereas Si^{4+} and Fe^{3+} can substitute for one another in tetrahedral sites. We hypothesize that aqueous fluids facilitated the reaction.

Reaction 1 can theoretically progress in either direction, although evidence from studies on CM matrix provides additional insight. The Fe/Si ratio in the matrix of CM chondrites decreases with increasing degree of alteration, which McSween (1979) suggested resulted from the formation of phyllosilicate phases containing higher Mg/Fe ratios. Tomeoka and Buseck

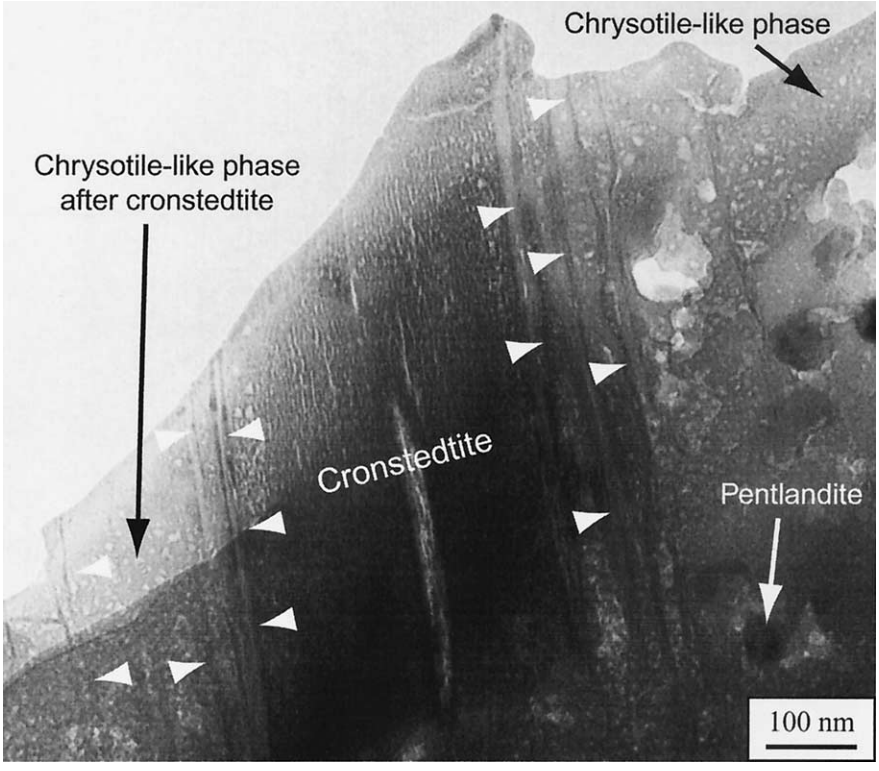

Fig. 4. TEM image of the chrysotile-like phase and pentlandite-bearing region separated by cronstedtite. The relict cronstedtite layers are indicated (white arrowheads). The chrysotile-like phase partially replaces cronstedtite (lower-left region of image).

Table 3. Average mineral compositions from focused and defocused beam (50 to 1000 nm) TEM-EDS measurements (normalized to 100 at %).[a]

Element	Chrysotile-like (16)[b]		Cronstedtite (22)[e]		Polygonal Serpentine (3)[b]		Pentlandite (6)	
Mg	11.6	*1.5*	4.2	*1.6*	14.2	*0.9*	BMDL	—
Al	0.6	*0.4*	1.9	*0.4*	BMDL	—	BMDL	—
Si	10.9	*0.8*	8.8	*0.8*	11.2	*0.2*	BMDL	—
Fe^{2+}	4.1	*1.3*	9.4	*1.8*[f]	2.3	*1.4*	25.4	*2.0*
Fe^{3+}	—	—	3.8	—	—	—	—	—
Ni	0.1	*0.2*	BMDL	—	BMDL	—	28.6	*1.6*
S	0.6	*0.2*	0.4	*0.5*	BMDL	—	46.0	*1.6*
H[c]	23.0	—	21.4	—	22.4	—	—	—
O[d]	49.4	—	50.1	—	50.0	—	—	—

[a] Number of analyses included in average compositions are shown in parentheses. Numbers in italics indicate the standard deviations. BMDL = below minimum detection level.

[b] All Fe is assumed to be Fe^{2+}

[c] Hydrogen composition is calculated: H = 2*(Al + Si), in accordance with serpentine stoichiometry.

[d] Oxygen composition is calculated: O = Mg + 1.5*(Al + Fe^{3+}) + 2*Si + Fe^{2+} + Ni + 0.5* H − S, based on oxides of these cations minus S.

[e] Assumes Fe is 28.6% Fe^{3+} and 71.4% Fe^{2+}, in accordance with a partially substituted cronstedtite stoichiometry where x = 0.5.

[f] Standard deviation applies to total Fe.

(1985) expanded on this model and suggested that cronstedtite and serpentine reacted during advanced alteration to form Fe-bearing serpentine, which enriched the matrix in Mg. The chrysotile-like phase and polygonal serpentine contain the highest Mg/Fe ratios among the FGR minerals (Table 3, Fig. 9). Therefore, Reaction 1 probably proceeded from left to right. Any Fe that was released presumably contributed to the formation of tochilinite and pentlandite.

The structural disorder and defects that some cronstedtite grains exhibit can be explained by the effects of Reaction 1. The curled serpentine structure presumably results from dimensional misfit between octahedral and tetrahedral sheets (for a review of serpentine structures, see Wicks and O'Hanley, 1988). Strain from substitution of larger cations is accommodated through periodic inversion of tetrahedra and curving of the tetrahedral and octahedral sheets; polygonization is another aspect of this mechanism (Dodony, 1997). We therefore interpret the separation of cronstedtite layers at its boundaries (Fig. 6) as effects of its conversion to the chrysotile-like phase and polygonal serpentine. The surface layers of cronstedtite in contact with a fluid presumably became unstable; Fe^{3+} was replaced by Mg^{2+} and Si^{4+}, which caused layer separation and curling. We hypothesize that the edge dislocations occurring in kinked areas (Fig. 5b) resulted from similar effects.

Small, Mg-rich cylindrical serpentine grains were identified as the most abundant phase in the FGRs of the ALH 81002 CM chondrite by Lauretta et al. (2000), who suggested that conversion from cronstedtite to serpentine resulted in a grain-size reduction during aqueous alteration. Most of the chrysotile-like phase in the Cold Bokkeveld FGRs is finer grained than cronstedtite, which is consistent with the proposed reaction mechanism of Lauretta et al. (2000). Hanowski and Brearley (1996, 2001) indicate that alteration of chondrule olivine can also produce fine-grained serpentines. Reaction of cronstedtite to

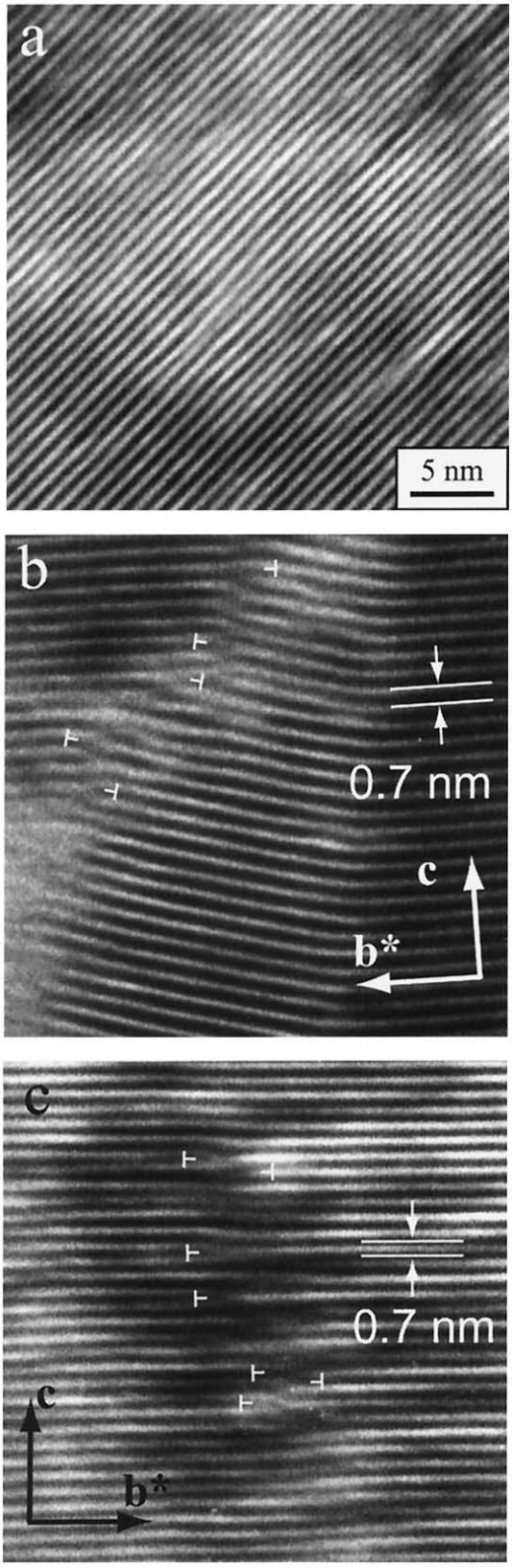

Fig. 5. (a) TEM image of a well-ordered region of a cronstedtite grain. (b,c) Other regions within the grain exhibit layer separation and contain kinks. Edge dislocations (⊥) occur parallel to the a-axis.

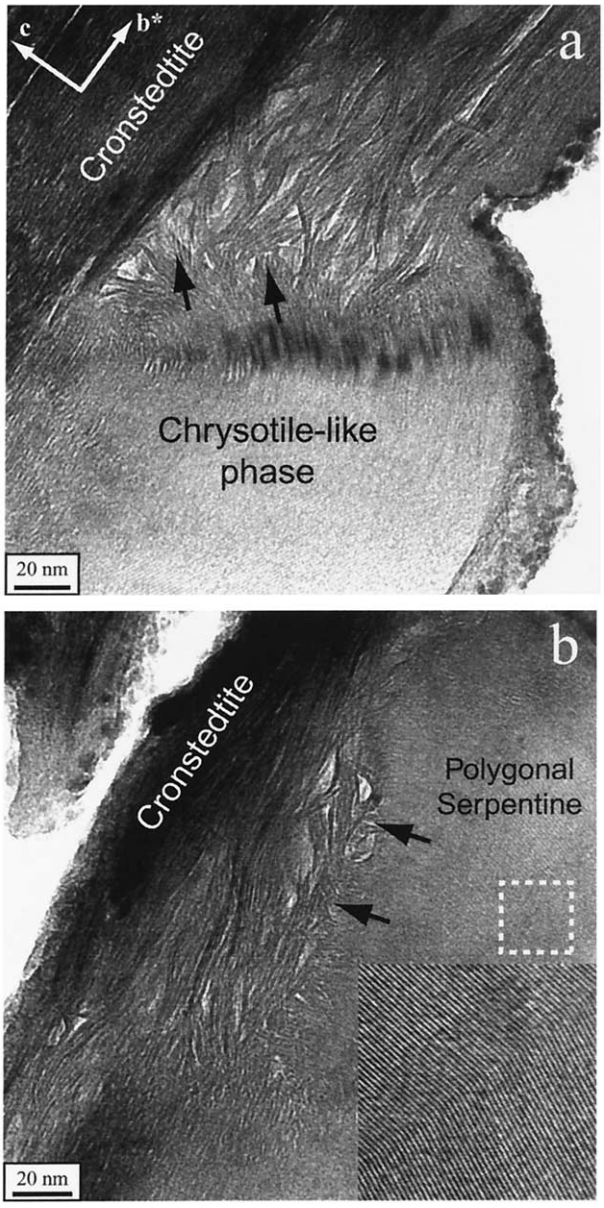

Fig. 6. TEM image of cronstedtite intergrown with (a) the chrysotile-like phase and (b) polygonal serpentine. Layers are disordered in the region between cronstedtite, the chrysotile-like phase, and polygonal serpentine. The black arrows indicate curling. (b) The sectors of polygonal serpentine (inset image) are best viewed by looking at the image at a shallow angle.

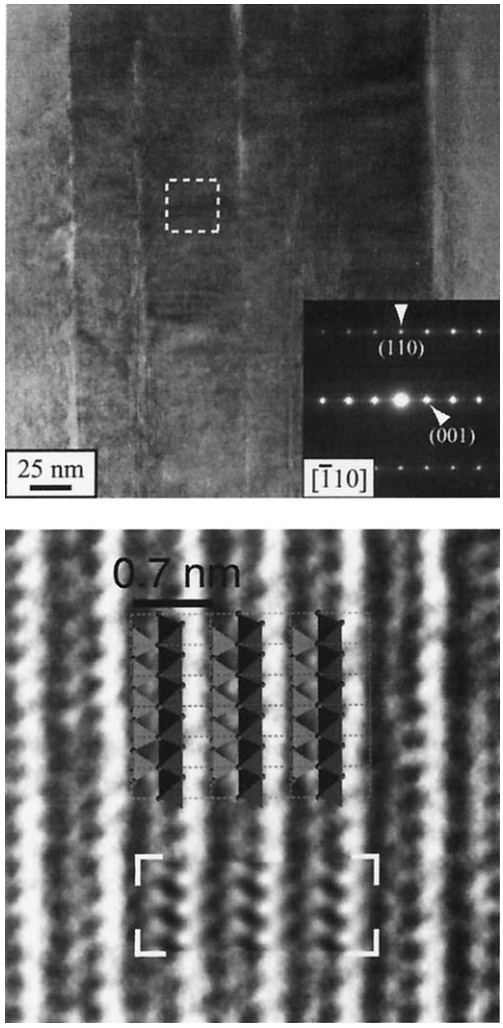

Fig. 7. TEM image of cronstedtite. The lower image is an enlargement of the white-boxed region from the top image, together with two insets, an image simulation (white brackets), and polytype 1*T* structure model. The match between the simulated (7.6-nm thickness, $\Delta f = -60.8$ nm) and experimental images allows identification of the octahedral and tetrahedral sheets (dark and light-gray bands, respectively). The SAED pattern (top, inset) is of the entire cronstedtite grain.

serpentine is evidently one of several alteration pathways by which fine-grained material was produced in the CM chondrites.

4.2. Cosmochemical Implications

Non-uniform FGR widths were observed in other CM chondrites (Metzler et al., 1992; Metzler and Bischoff, 1997; Bischoff, 1998; Hua et al., 2002). The explanation proposed for such features is that material accreted onto the surface of chondrules and filled in the embayed areas. Our data are consistent with this interpretation. Also, the Cold Bokkeveld FGRs exhibit sedimentary textures such as layering and grain-size coarsening outward from the chondrules they enclose, similar to textures described for other CM chondrites (Brearley and Geiger, 1991, 1993; Metzler et al., 1992) and interpreted as primary nebular features (Brearley et al., 1999). The layering of these Cold Bokkeveld FGRs (e.g., Fig. 1e,f) is best explained by accretion episodes in which coarser dust was deposited onto finer dust.

Preaccretionary alteration scenarios, based on a variety of textural and mineralogic data, were proposed for a major portion of the hydrous material in the FGRs and matrix of CM chondrites (Metzler et al., 1992; Bischoff, 1998). In their TEM study of the FGRs of ALH 81002, Lauretta et al. (2000) observed anhydrous olivine and metal grains in direct contact with phyllosilicates and interpreted it, plus the variable extent of alteration in the FGRs, as evidence consistent with the

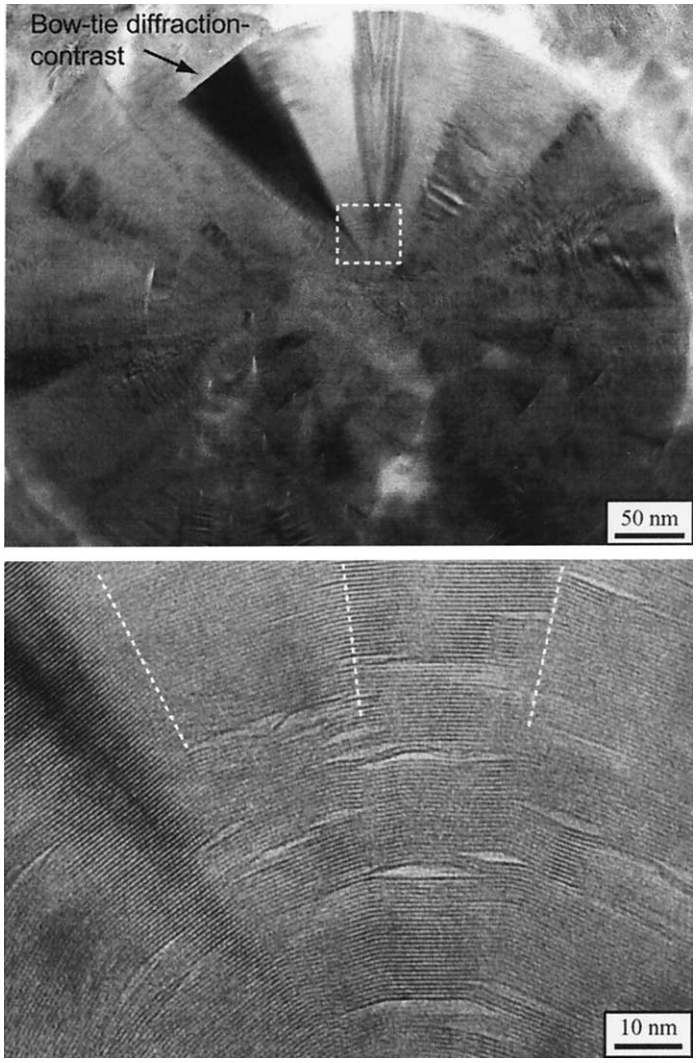

Fig. 8. TEM image of polygonal serpentine. The top image illustrates the characteristic bow-tie diffraction-contrast of polygonal serpentine. The bottom image exhibits the separation of layers occurring near and between sector boundaries (dotted white lines).

preaccretionary alteration model of Metzler et al. (1992). However, both Hanowski and Brearley (2001) and Hua et al. (2002) suggested that the FGRs and chondrules of ALH 81002 were altered on a parent body, based on the similar compositions and textures among FGR, chondrule alteration, and vein material.

The relative uniformity of the mineralogy and average compositions of the Cold Bokkeveld FGRs indicate that they experienced similar types and extents of alteration. The Mg/(Mg+Fe) ratios of cronstedtite grains among the FGRs indicate comparable degrees of Mg substitution. The cronstedtite from the Cold Bokkeveld FGRs is more Mg-rich than that from Murchison (Brearley et al., 1999) but similar to grains from ALH 81002 (Lauretta et al., 2000). These observations are compatible with the parent-body-alteration model of Brearley et al. (1999) in which rim phyllosilicates experienced progressive equilibration with a Mg-rich fluid.

Based on veins of calcium sulfate that fill matrix-cutting fractures, Lee (1993) suggested that Cold Bokkeveld experienced aqueous alteration on the parent body. The depletion of Ca in the FGRs (Fig. 2) can be explained by parent-body aqueous alteration (Hua et al., 2002). Ca could have been mobilized during such alteration, transported away from the FGRs, and precipitated as carbonates or sulfates in the matrix (Barber, 1981; Lee, 1993).

Metal and anhydrous silicates occur in direct contact with sheet silicates in the FGRs of ALH 81002 (Lauretta et al., 2000). In contrast, the Cold Bokkeveld FGRs contain predominantly hydrous minerals, indicating more intense alteration than the FGRs of ALH 81002. Lauretta et al. (2000) proposed that aqueous alteration of cronstedtite to serpentine produced decreases in grain sizes in the FGRs of ALH 81002. We find similar evidence in the Cold Bokkeveld FGRs. However, the data from the Cold Bokkeveld FGRs point toward parent-body alteration, whereas preaccretionary alteration was concluded as more likely for the FGRs of ALH 81002. The similar bulk compositions and mineralogies reported among the ALH 81002 FGRs could also be consistent with parent-body alteration, as

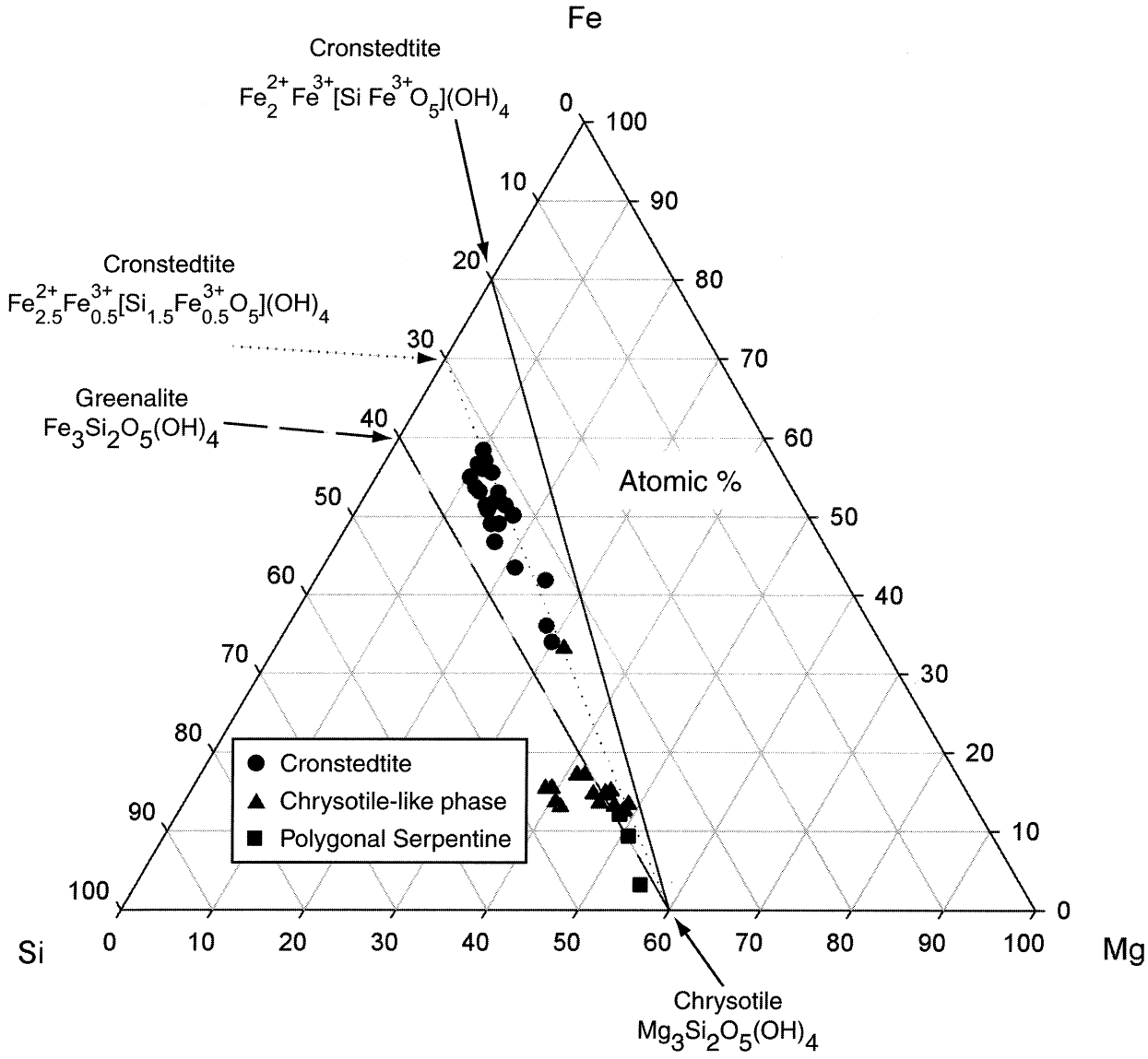

Fig. 9. Mg-Fe-Si ternary plot of the Cold Bokkeveld FGR mineral compositions as quantified from EDS measurements (at %). Mixing lines between endmember chrysotile and cronstedtite (solid), partially substituted cronstedtite (dotted), and greenalite (dashed) compositions are plotted.

suggested by Hanowski and Brearley (2001) and Hua et al. (2002). The variable extent of alteration reported in the FGRs of ALH 81002 could be explained if (1) alteration reactions were not driven to completion, (2) certain minerals were shielded from altering fluids, (3) alteration varied according to relative solubilities and surface areas, or (4) some combination of these variables occurred.

The data from Murchison (Brearley and Geiger, 1991, 1993) and the Cold Bokkeveld silicates (present study) and sulfate veins (Lee, 1993) indicate that aqueous alteration of these CM meteorites occurred on the parent body, just as evidence from other CM chondrites suggests aqueous alteration occurred before accretion of the FGRs (Metzler et al., 1992; Bischoff, 1998). However, rather than being an either/or situation for the CM chondrites as a group as has been widely assumed, it seems plausible that aqueous alteration of some meteorites could have occurred before accumulation, and others like Cold Bokkeveld were altered on the parent body, with the details depending on the particular meteorite.

5. CONCLUSIONS

1. The FGRs around chondrules in the Cold Bokkeveld CM chondrite are dominated by hydrous minerals and pentlandite. TEM and EDS data indicate reaction among cronstedtite, the chrysotile-like phase, and polygonal serpentine.
2. Cronstedtite grains exhibit layer separation, particularly at boundaries with the chrysotile-like phase and polygonal serpentine that presumably resulted from the effects of aqueous alteration.
3. EDS data from cronstedtite grains indicate comparable degrees of Mg substitution among the FGRs. The cronstedtite

from Cold Bokkeveld is more Mg-rich than that from Murchison (Brearley et el., 1999).

4. TEM evidence suggests that the alteration of cronstedtite to the chrysotile-like phase was accompanied by a reduction in grain size, which is consistent with a similar effect in the FGRs of the ALH 81002 CM chondrite, as shown by Lauretta et al. (2000).
5. The Cold Bokkeveld FGRs surround different types of chondrules, have similar bulk compositions, exhibit nonuniform thicknesses, layering, and grain-size coarsening outward from the chondrules they enclose. These characteristics are similar to FGRs of other CM chondrites.
6. The data are consistent with accretion of dust onto chondrules, presumably in the solar nebula, and subsequent aqueous alteration on the parent body.

Acknowledgments—We thank Carleton Moore and the Center for Meteorite Studies for providing the sample of Cold Bokkeveld, and we thank Jim Clark and John Wheatley for EMPA and TEM assistance, respectively. We thank István Dódony for the insight that he provided on serpentine structures, and we thank Laurence A. J. Garvie, Craig L. Johnson, Hiromi Konishi, and John W. Moreau for discussions regarding TEM and mineralogy. We thank David R. Bell for discussions of compositional data and Xin Hua and Dante S. Lauretta for sharing their knowledge of cosmochemistry and for their initial editing of the manuscript. A. Bischoff, A. Brearley, and F. Brenker provided constructive reviews that greatly improved the manuscript. This work was supported in part by NASA grant NAG5-9352, a NASA Space Grant Fellowship, Arizona Mining and Mineral Museum Scholarship, and Sigma Xi grant-in-aid of research.

Associate editor: H. Palme

REFERENCES

Barber D. J. (1981) Matrix phyllosilicates and associated minerals in C2M carbonaceous chondrites. *Geochim. Cosmochim. Acta* **45,** 945–970.

Bischoff A. (1998) Aqueous alteration of carbonaceous chondrites: Evidence for preaccretionary alteration–A review. *Meteorit. Planet. Sci.* **33,** 1113–1122.

Brearley A. J. (1993) Matrix and fine-grained rims in the unequilibrated CO3 chondrite, ALHA 77307: Origins and evidence for diverse, primitive nebular dust components. *Geochim. Cosmochim. Acta* **57,** 1521–1550.

Brearley A. J. and Geiger T. (1991) Mineralogical and chemical studies bearing on the origin of accretionary rims in the Murchison CM2 carbonaceous chondrite. *Meteoritics* **26,** 323.

Brearley A. J. and Geiger T. (1993) Fine-grained chondrule rims in the Murchison CM2 chondrite: Compositional and mineralogical systematics. *Meteoritics* **28,** 328–329.

Brearley A. J., Bajt S., and Sutton S. R. (1995) Distribution of moderately volatile trace elements in fine-grained chondrule rims in the unequilibrated CO3 chondrite, ALH A77307. *Geochim. Cosmochim. Acta* **59,** 4307–4316.

Brearley A. J., Hanowski N. P., and Whalen J. F. (1999) Fine-grained rims in CM carbonaceous chondrites: A comparison of rims in Murchison and ALH 81002. *Lunar Planet. Sci.* **XXX,** 1460.

Browning LB., McSween H. Y. Jr., and Zolensky ME. (199) Correlated alteration effects in CM carbonaceous chondrites. *Geochim. Cosmochim. Acta* **60,** 2621–2633.

Bunch T. E. and Chang S. (1984) CAI rims and CM2 dustballs: Products of gas-grain interactions, mass transport, grain aggregation and accretion in the nebula? *Lunar Planet. Sci.* **XV,** 100–101.

Buseck P. R., Devouard B., and Hua X. (1997) Comparison of the mineralogy of fine-grained rims and adjacent matrix in CM2 chondrites. *Meteorit. Planet. Sci.* **32,** A24–-A25..

Cliff G. and Lorimer G. W. (1975) The quantitative analysis of thin specimens. *J. Microscopy* **103,** 203–207.

Dódony I. (1997) Structure of the 30-sectored polygonal serpentine. A model based on TEM and SAED studies. *Phys. Chem. Miner.* **24,** 39–49.

Geiger C. A., Henry D. L., and Bailey S. W. (1983) Crystal structure of cronstedtite-2H_2. *Clay. Clay Miner.* **31,** 97–108.

Hanowski N. P. and Brearley A. J. (1996) Chondrule alteration in the CM carbonaceous chondrite, LEW 90500. *Lunar Planet. Sci.* **XXVII,** 487–488.

Hanowski N. P. and Brearley A. J. (2001) Aqueous alteration of chondrules in the CM carbonaceous chondrite, Allan Hills 81002: Implications for parent body alteration. *Geochim. Cosmochim. Acta* **65,** 495–518.

Hua X., Zinner E. K., and Buseck P. R. (1996) Petrography and chemistry of fine-grained dark rims in the Mokoia CV3 chondrite: Evidence for an accretionary origin. *Geochim. Cosmochim. Acta* **60,** 4265–4274.

Hua X., Wang J., and Buseck P. R. (2002) Fine-grained rims in the ALH81002 and LEW90500 CM2 meteorites: Their origin and modification. *Meteorit. Planet. Sci.* **37,** 229–244.

Hybler J., Petrcek V., Durovic S., and Smrcok L. (2000) Refinement of the crystal structure of cronstedtite-1*T. Clay. Clay Miner.* **48,** 331–338.

Kerridge J. F. and Matthews M. S. (1988) Appendix 3. In *Meteorites and the Early Solar System* (eds. J. F. Kerridge and M. S. Matthews), pp. 1197, University of Arizona Press.

Lauretta D. S., Hua X., and Buseck P. R. (2000) Mineralogy of fine-grained rims in the ALH 81002 CM chondrite. *Geochim. Cosmochim. Acta* **64,** 3263–3273.

Lee M. R. (1993) The petrography, mineralogy and origins of calcium sulphate within the Cold Bokkeveld CM carbonaceous chondrite. *Meteoritics* **28,** 53–62.

Li J., Hua X., and Buseck P. R. (1999) Mineralogy of fine-grained rims in LEW90500 by transmission electron microscopy. *Lunar Planet. Sci.* **XXX,** 1271.

McSween H. Y. Jr. (1979) Alteration in CM carbonaceous chondrites inferred from modal and chemical variations in matrix. *Geochim. Cosmochim. Acta* **43,** 1761–1770.

Metzler K. and Bischoff A. (1997) Constraints on chondrite agglomeration from fine-grained chondrule rims. In *Chondrules and the Protoplanetary Disk* (eds. R. H. Hewins, R. H. Jones, and E. R. D. Scott), pp. 153-161, Cambridge University Press.

Metzler K., Bischoff A., and Stoffler D. (1992) Accretionary dust mantles in CM chondrites: Evidence for solar nebula processes. *Geochim. Cosmochim. Acta* **56,** 2873–2897.

Müller W. F., Kurat G., and Kracher A. (1979) Chemical and crystallographic study of cronstedtite in the matrix of the Cochabamba (CM2) carbonaceous chondrite. *Tschermaks Miner. Petrog.* **26,** 293–304.

Sears D. W. G., Jie L., and Benoit P. H. (1992) Chondrule rims in Murchison, cathodoluminescence evidence for in situ formation by aqueous alteration. *Meteoritics* **27,** 288.

Sears D. W. G., Benoit P. H., and Jie L. (1993) Two chondrule groups each with distinctive rims in Murchison recognized by cathodoluminescence. *Meteoritics* **28,** 669–674.

Smrcok L., Durovic S., Petricek V., and Weiss Z. (1994) Refinement of the crystal structure of cronstedtite-3T. *Clay. Clay Miner.* **42,** 544–551.

Tomeoka K. and Buseck P. R. (1985) Indicators of aqueous alteration in CM carbonaceous chondrites: Microtextures of a layered mineral containing Fe, S, O and Ni. *Geochim. Cosmochim. Acta* **49,** 2149–2163.

Van Cappellen E. and Doukhan J. C. (1994) Quantitative transmission X-ray microanalysis of ionic compounds. *Ultramicroscopy* **53,** 343–349.

Wicks F. J. and O'Hanley D. S. (1988) Serpentine minerals: Structures and petrology. In *Hydrous Phyllosilicates* (ed. S. W. Bailey), *Rev. Mineral.* **19,** pp. 91–167.

Wicks F. J. and Plant A. G. (1979) Electron-microprobe and X-ray-microbeam studies of serpentine textures. *Can. Mineral.* **17,** 785–830.

Zega T. J. and Buseck P. R. (2000) Mineralogy of a fine-grained rim within the Cold Bokkeveld CM chondrite: A TEM study. *Meteorit. Planet. Sci.* **35,** A177.

Zega T. J. and Buseck P. R. (2001) Fine-grained rim mineralogy of the Cold Bokkeveld CM chondrite. *Meteorit. Planet. Sci.* **36,** A230.

Zolensky M. E., Barrett R., and Browning L. (1993) Mineralogy and composition of matrix and chondrule rims in carbonaceous chondrites. *Geochim. Cosmochim. Acta* **57,** 3123–3148.